CHAPTER 6

MORPHOLOGICAL TRANSFORMATION IN Au-Cu ALLOY NANOPARTICLES

In this chapter, evolution of growth morphology of resulting alloys by changing the concentration of stabilizer and Cu precursor is presented. Two distinct growth morphologies of Au-Cu have been observed. They refer to multipods and nanowires. This chapter begins with some introductory remarks and experimental details. Following this, results are presented and discussed. Conclusions drawn from this part of investigations are given at the end.

6.1 Introduction

The synthesis of bimetallic NPs with desired shape and composition seems to be a difficult task owing to the nature of nucleation and growth processes. Literature on the synthesis of specified shape and chemistry of Au–Cu bimetallic NPs is scarce [223–225]. Liu and Walker synthesized Au–Cu alloy nanocubes employing polyol method [223]. They showed that size and composition of the nanocubes influenced the LSPR behaviour significantly. Chen et al. grew intermetallic Au–Cu NPs by allowing Cu atoms to diffuse into pre-synthesized Au seeds [224]. Atomic-scale diffusion in solution phase is homogeneous and generates uniform and monodisperse products compared to solid state diffusion. In spite of some important studies of Au–Cu bimetallic NPs in well-defined shape, control of

facets of NPs remains a challenging task. For example, there are limited reports on low-index facets like {111}, {100} and {110}. Controlling the nature of exposed surfaces and facets of NPs directly dictates their properties. There is a continuous push for engineering interesting shapes, for instance, NPs with multiple branches. In general, highly branched NPs possess increased surface-to-volume ratio. Further, rough surfaces in comparision to their smooth counterparts, may be utilized in surface-sensitive applications such as LSPR and catalysis [226–228]. It has also been observed that branched nanostructures are often exposes high-index facets [229–232]. These lower symmetric facets relate to a high density of atomic steps, kinks and edges with low coordination numbers, which can act as highly active sites for breaking chemical bonds [228–231]. It is important to mention here that limited success has been achieved in the synthesis of alloy NPs with multiple branches. Hence, it may be rewarding to explore the synergy between Au, Cu and branched shape on the LSPR behavior. Therefore, one of the goals of this chapter is to synthesize and understand the growth process of branched Au–Cu nanostructures as well as to study their LSPR behavior which may pave the way for potential applications in photo-thermal therapy. Another interesting morphology of technological importance is one-dimensional nanostructures such as nanowires. As mentioned in chapter 1,there are two main mechanisms by which anisotropic shapes evolve in the growth process. The classical Ostwald ripening (OR) and oriented attachment (OA) mechanism [33, 34]. The colloidal NPs form through nucleation, followed by a growth process in which ad-atoms are consumed [233–237]. Recently, in-situ transmission electron microscopy (TEM) studies show that final resulting NPs can be generated from the primary colloidal nanoclusters

[238, 239]. In some cases, primary particles can grow into nanowires through oriented attachment [35–39, 240–243]. For semiconducting quantum dots and oxides, dipolar interaction seems to the key driving force for the formation of such nanowires. The oriented attachment however can lead to the formation of low dimensional morphologies in materials with no permanent dipole as well [40], suggesting factors other than dipolar interaction may also be important. The effect of concentration of stabilizer hexadecylamine (HDA) and Cu ions on growth morphology of Au-Cu anisotropic nanostructures is presented in this chapter. In addition, mechanistic studies pertaining to growth of Au-Cu nanowires has also been discussed.

6.2 Experimental details

Forty five mg of HDA was mixed in 4.0 mL of deionized water with the help of ultrasonicator for about 1.0 h till complete mixing. In this emulsion, 0.3 mL (0.1 M) $CuCl_2.2H_2O$ and 0.3 mL (0.1M) $HAuCl_4.3H_2O$ was added and stirred magnetically for 10 minutes at room temperature. A light green color solution was observed.This solution was placed in an oil bath maintained at $\sim 80^oC$ for about 15 minutes and a light blue color appears within several minutes. At this point 0.3 mL (1.0 M) freshly prepared glucose solution was added in hot condition and capped the vial.After 2-3 minutes, the blue color changed to light purple and within a few minutes transformed to black color. This was continued for 10 minutes. The vial was taken out from the oil bath and cooled to room temperature. Aliquotes were taken out after 2 min, 4 min, and 6 min respectively after glucose was added into the reaction vial. The samples were cleaned by repeated addition of n-hexane

and ethanol followed centrifugation and ultrasonication cycles. The powder thus obtained was dispersed in n-hexane and a drop was coated on TEM grid (carbon coated Ni-grid with mesh size 400). The morphology and structures were investigated by TEM (FEI Tecnai G^2 T20, operating at 200 kV). The average chemistry of the grown nanostructures was probed by HAADF-STEM-EDS. The LSPR behaviour of sols was studied by UV-Vis spectrometer (Agilent Cary UV-Vis and Perkin-Elmer Lambda XLS+).

6.3 Results and discussion

6.3.1 Growth of Au-Cu multipod nanostructures

Growth morphology was followed by TEM with varying the amount of capping agent (45 mg, 90 mg, 135 mg and 190 mg of HDA) while kept all other reaction parameters nearly same. Figure 6.1 (a) displayed branched Au-Cu nanostructures when the HDA concentration was 45 mg. The appearance of bipod, tripod and tetrapod nanostructures were seen. In other cases, wire-like features associated with many nodes and stems have been observed. For example, when HDA was kept at 90 mg the nanowires with average width $\sim$ 6.0 nm and length $\sim$ 90 nm have been observed. The SAD patterns for both branched and wires nanostructures are shown in Figure 6.2 (a) and (b) respectively. The rings could be indexed systematically and phase was found to be those of FCC- AuCu.

The possible mechanism for the formation of multipods can be explained as the following. At the beginning of reaction $AuCl_4^-$ and Cu^{2+} reduced quickly to Au and Cu by glucose. This especially applies to $AuCl_4^-$, because of the apparently higher redox

potential of $AuCl_4^-$ than Cu^{2+}. Fast reduction gave rise to the formation of a large number of small seeds. It was pointed out by Yacaman et al.[244] that at nanometric sizes,the fivefold twinned structures such as icosahedrons and decahedrons tend to be more stable than cuboctahedrons [244–246]. As a result of this multiply twinned seeds can form due to thermodynamic preference. The concentration of $AuCl_4^-$ ions in the suspension went down very fast due to their faster reduction, whereas Cu^{2+} ions concentration was maintained at relatively high level. The multiply twinned particles grew intially but such a

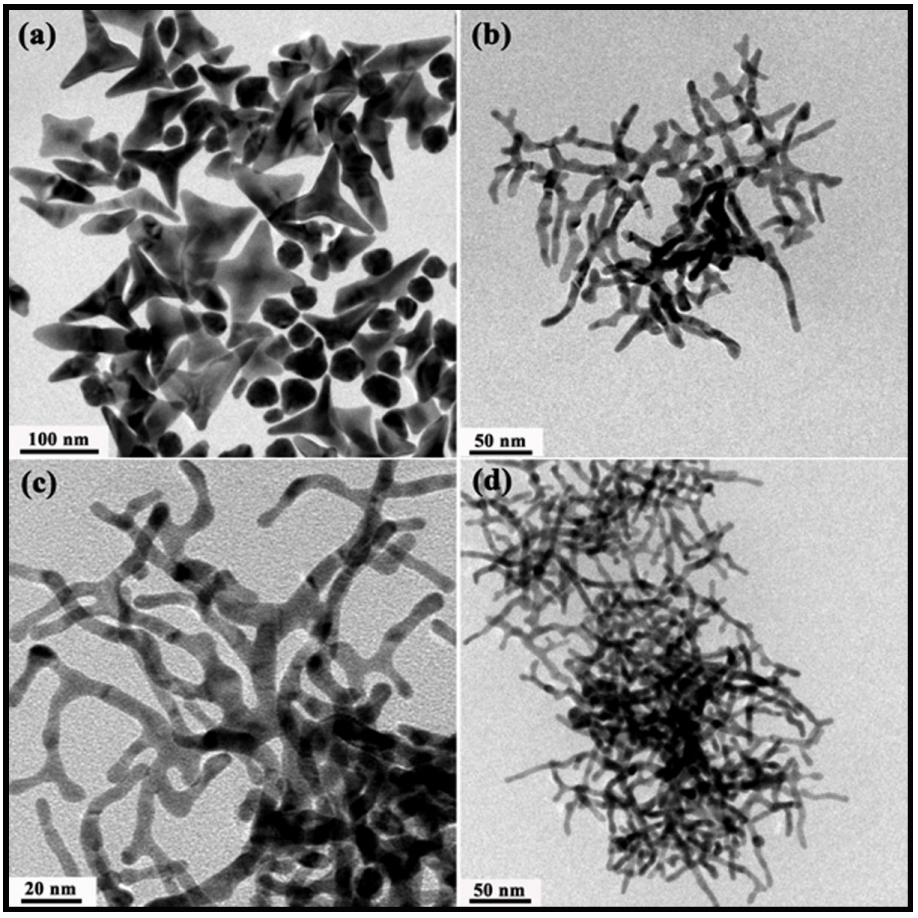

FIGURE 6.1: Representative TEM images of Au-Cu nanostructures with varying HDA concentration. Figures (a), (b), (c), and (d) corresponds to HDA concentration of 45 mg, 90 mg, 135 mg and 180 mg, respectively.

growth could not be sustained further owing to change in nature of growth process. Subsequent attachment of reduced metal atoms took place at twinning planes due to high energy sites rather on facets [125]. This preferential deposition could be attributed to the underpotential deposition of Cu on Au seeds [247]. The twin boundaries observed in tripod and tetrapod nanostructures are shown in Figure 6.3. The predominant attachments of metal atoms along the twinning planes of multiply twinned seeds led to the formation multipods. The chemistry of the Au-Cu multipods was investigated by HAADF-STEM-EDS and average composition was found to be $\sim$ 77 at. % Au and $\sim$ 23 at. % Cu respectively. The STEM-EDS elemental maps shown in Figure 6.4 depicted uniform distribution of Au and Cu throughout the tripod and tetrapod features suggested that Au-Cu alloy has been formed.The lattice parameter of FCC-AuCu solid solution was found to be $\sim$ 3.97Å based on Vegard's law.

In order to probe the influence of Cu ions in the formation of multipods, an

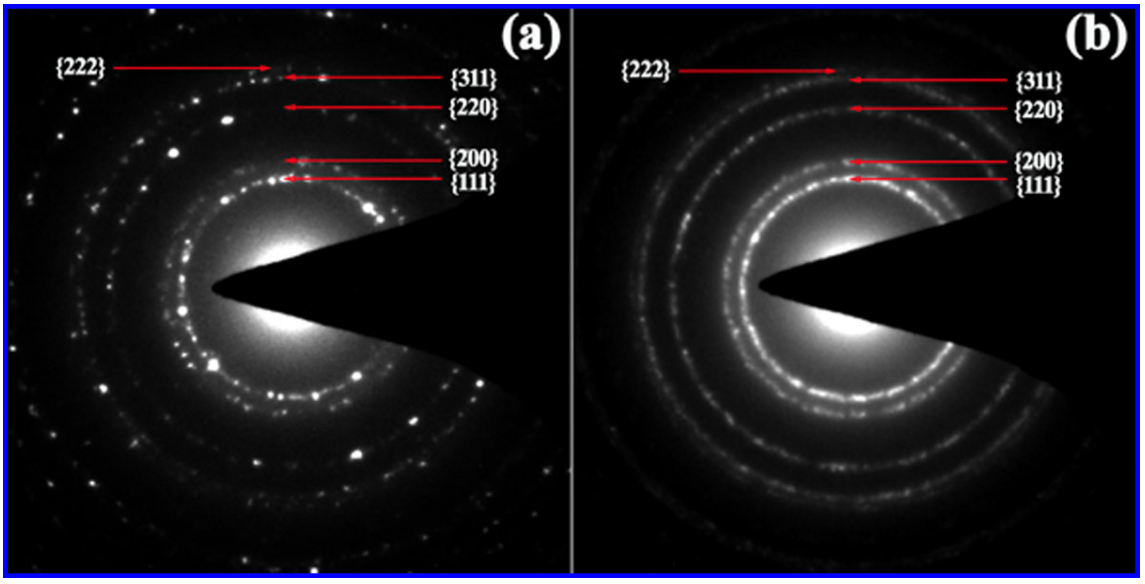

FIGURE 6.2: Selected area diffraction patterns from Au-Cu (a) nanopods and (b) nanowires.

experiment was conducted without Cu precursor in the standard protocol (45 mg HDA). The morphology and corresponding SAD pattern is presented in Figure 6.5 (a) and (b) respectively. A HRTEM image of a particle shown as inset in Figure 6.5 (a) displays twins. This is in conformity with previously discussed growth mechanism of multipods where growth takes place along twin planes. The TEM image shows that nearly spherical NPs of average size $\sim$ 8.0 nm have formed. The DP was indexed and phase was found to those of FCC Au. Absence of morphological anisotropy points out that presence of Cu ions seems to play a substantial role in promoting the anisotropy in Au-Cu nanostructures in the present synthesis conditions. The role of Cu in promoting anisotropy in Au-Cu system has been delibereted in literature [248]. The experiments were also designed to investigate the role of precursors molar ratio (Au/Cu) on the growth morphology of the nanostructures while keeping the HDA amount fixed to 90 mg. Figure 6.6 depicts the TEM images showing morphology with changing the precursors molar ratio Au/Cu as

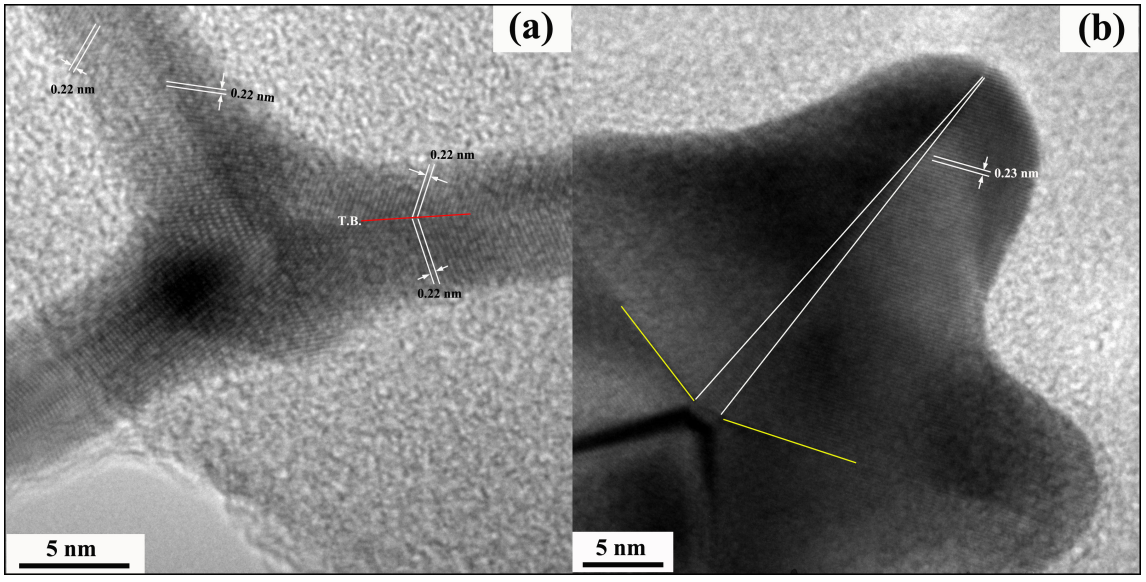

FIGURE 6.3: Representative HRTEM images of Au-Cu tripod (a) and tetrapod (b).

1/0, 2/1, 3/1, and 1/2 respectively. The wire-like features with nodes and stems have been observed in all the samples except Au/Cu (2/1) where multipods formed.

The SAD patterns in all the cases could be indexed to those of FCC-AuCu solid solution. Based on the above observations, it may be said that here ratio of Au precursor to HDA appears to play important role for the formation of Au-Cu multipods. The HAADF image and STEM-EDS spectrum of Au-Cu nanowires is displayed in Figure 6.7. The presence of both Au and Cu in nanowires indicating the formation of an Au–Cu

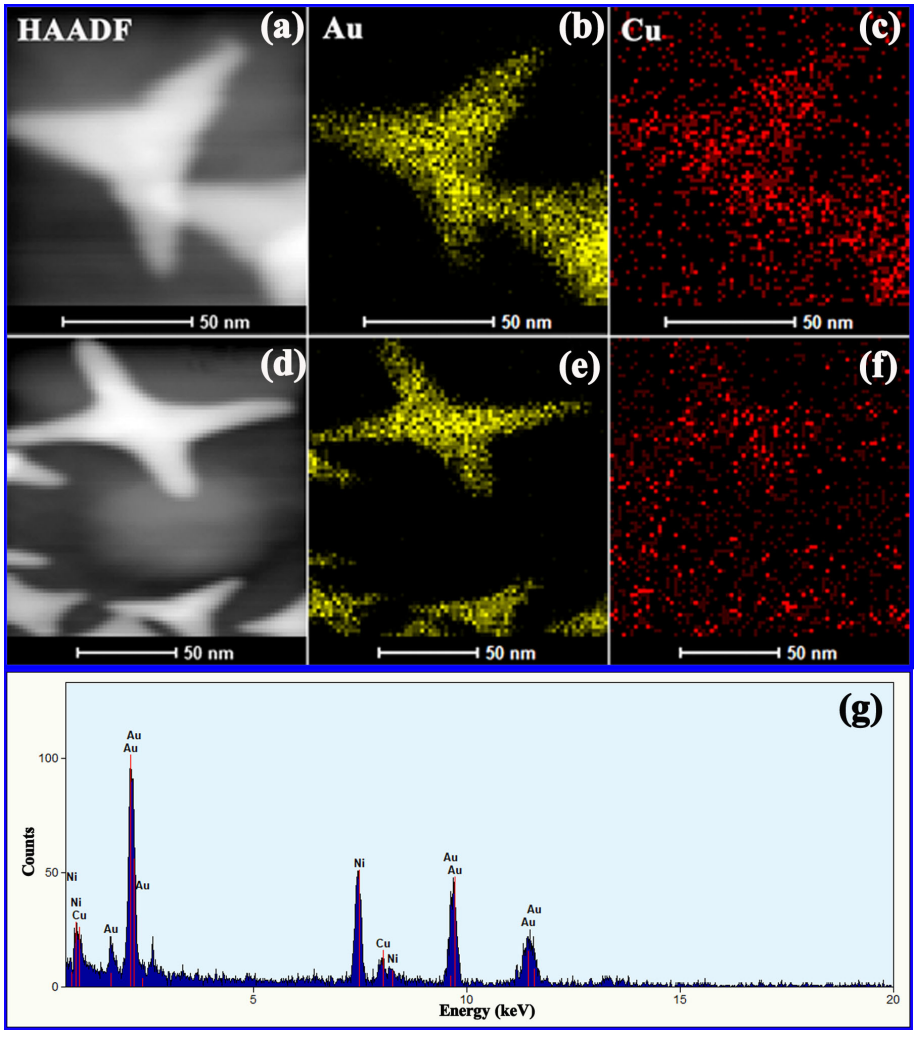

FIGURE 6.4: STEM-EDS elemental maps of tripod (a- c) and tetrapod (d- f) Au-Cu nanostructutes. Figure (g) shows EDS spectrum of Au-Cu nanostructures.

alloy phase. The average composition of Au and Cu was found to be $\sim$ 52 at. % and $\sim$ 48 at. % respectively. The lattice parameter was derived to be $\sim$ 3.85Å by invoking Vegard's law.

6.3.2 Formation of Au-Cu nanowires

The Au-Cu nanowires was observed when experiments were conducted with molar precursors ratio and HDA concentration as Au /Cu (1/1) and 90 mg onwards. Therefore, interrupted growth experiments were carried out to decipher the growth mechanism of the Au-Cu nanowires keeping HDA concentration to 90 mg. The aliquots were taken out after 2 min, 4 min, 6 minutes and 10 minutes after addition of glucose. The evolution of growth morphology was followed with TEM and images have been shown in Figure 6.8 (a) to (d). In 2 min sample, nanowires with many nodes and stems having average width $\sim$ 4 nm and length of $\sim$ 200 nm were seen. In addition, NPs of the average size

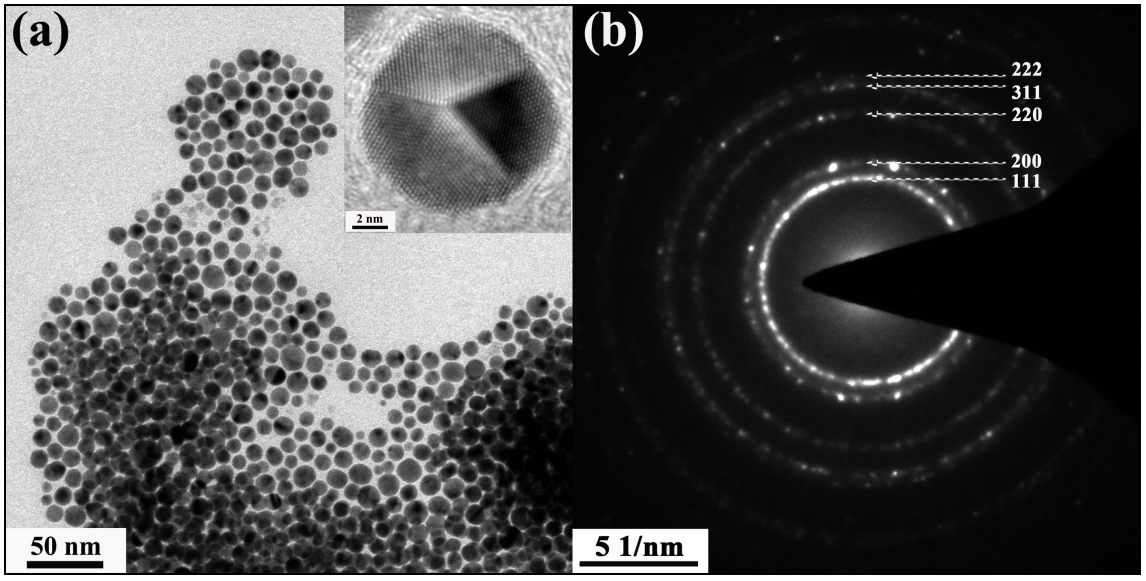

FIGURE 6.5: Reperentative TEM image with HRTEM from a particle as inset (a) and corresponding diffraction pattern (b) respectively, of Au NPs.

$\sim$ 3 nm were also observed. As the growth proceeds further, particle density decreased and more nodes and stems were observed in 4 min grown sample. The average width and length was measured to be $\sim$ 5 nm and 100 nm respectively. The average particle size in this case was found to be $\sim$ 5 nm. In 6 min grown sample, the average width and length of the nanowires was observed to be $\sim$ 7.0 nm and 70 nm respectively and finally after 10 min of growth no significant change in the dimensions of the nanowires was noticed. The coexistence of nanowires and larger size of the NPs as the growth proceeds suggest that both Ostwald ripening and oriented attachment mechanism are operative in the

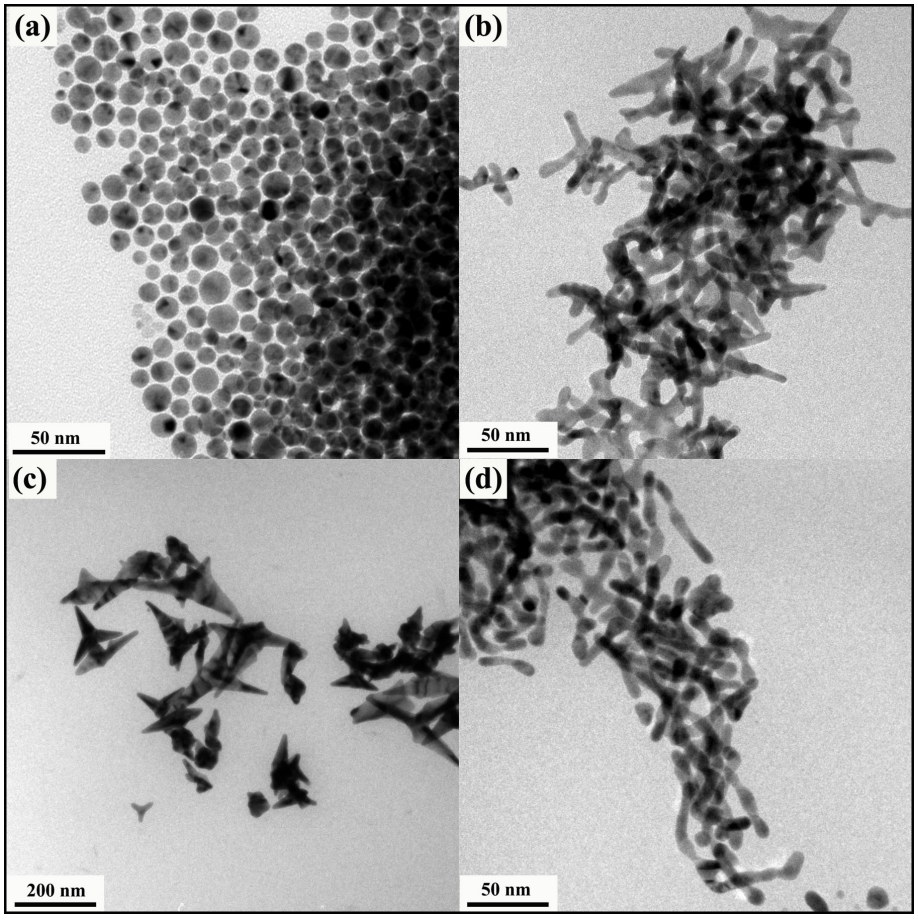

FIGURE 6.6: Growth morphologies of Au-Cu nanostructures by changing the molar precursors ratio of Au and Cu as (a) 1: 0, (b) 2:1, (c) 3:1 and (d) 1:2, respectively.

present synthesis conditions. To investigate the formation of nanowires, HRTEM is used to study the shape evolution of AuCu nanowires and the data show the attachment occurred mostly on {111} facets (Figure 6.9). Two growth modes, namely, lattice matched attachment (MA) and twinning attachment (TA) were observed [34]. Figures 6.9 (a) and (c) show attachments along {111} and {200} respectively. The grain boundary and lattice defect were not obvious if two primary particles attached and grew together via the

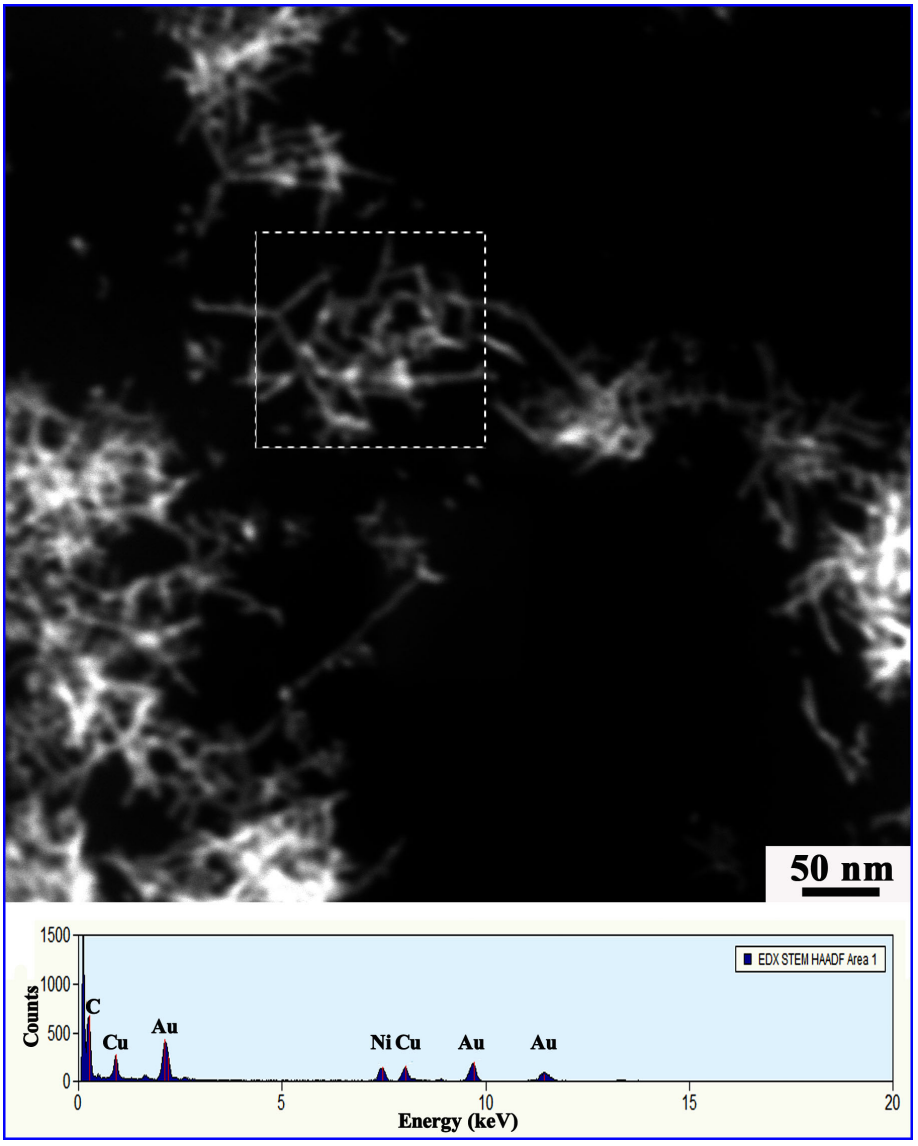

FIGURE 6.7: STEM-EDS spectrum of Au-Cu nanowires grown with Au:Cu (1:1) and HDA concentration of 90 mg.

MA mode. A twin plane with the mirror image like orientation could be observed if two particles attached through the TA growth on $\{111\}$ surfaces (Figure 6.9 b). Both linear and bending morphologies could be obtained when additional particles attached to the existing nanostructures through either MA or TA growth (Figure 6.9 d). The above experimental results indicate that the formation of AuCu nanowires was through the oriented attachment of primary NPs, which is different from those material systems that undergo anisotropic growth. In the latter case, the formation of twin planes in the seed crystals is a useful approach to the synthesis of nanowires [17, 249, 250]. For instance, the existence

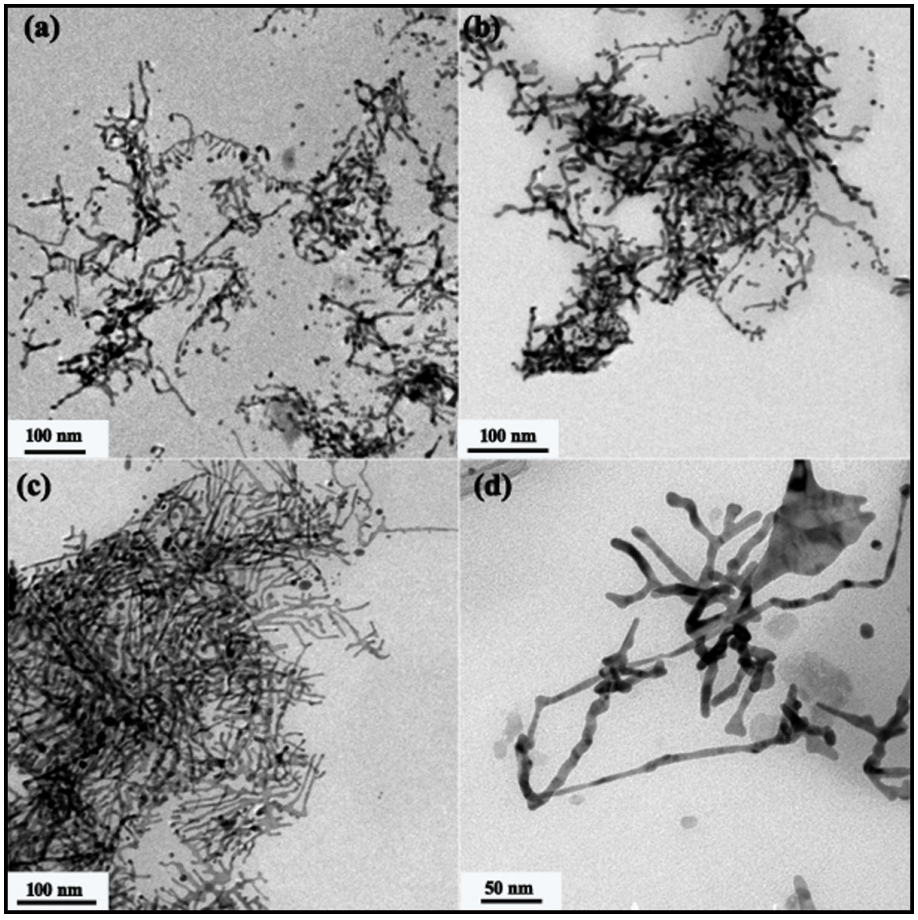

FIGURE 6.8: Growth morphology evolution of Au-Cu nanostructures after (a) 2 min, (b) 4 min, (c) 6 min and (d) 10 min respectively at fixed HDA proprtion of 90 mg with molar ratio of Au and Cu precursors as 1:1.

of 5-foldtwin plane in the seeds is important for reducing the symmetry of Ag NPs, when PVP is used as the capping agent [251]. These seeds led to the growth of nanowires. For oriented attachment however, defect is not necessary for the formation of low dimensional nanostructures. In a typical wet chemical method, the reduced precursors react to form seeds and subsequently grow into NPs. These NPs are stabilized by capping agents and move randomly in liquid phase. When two such NPs come close with each other, van der Waals forces begin to dominate in the interactions. If capping agents are present, they

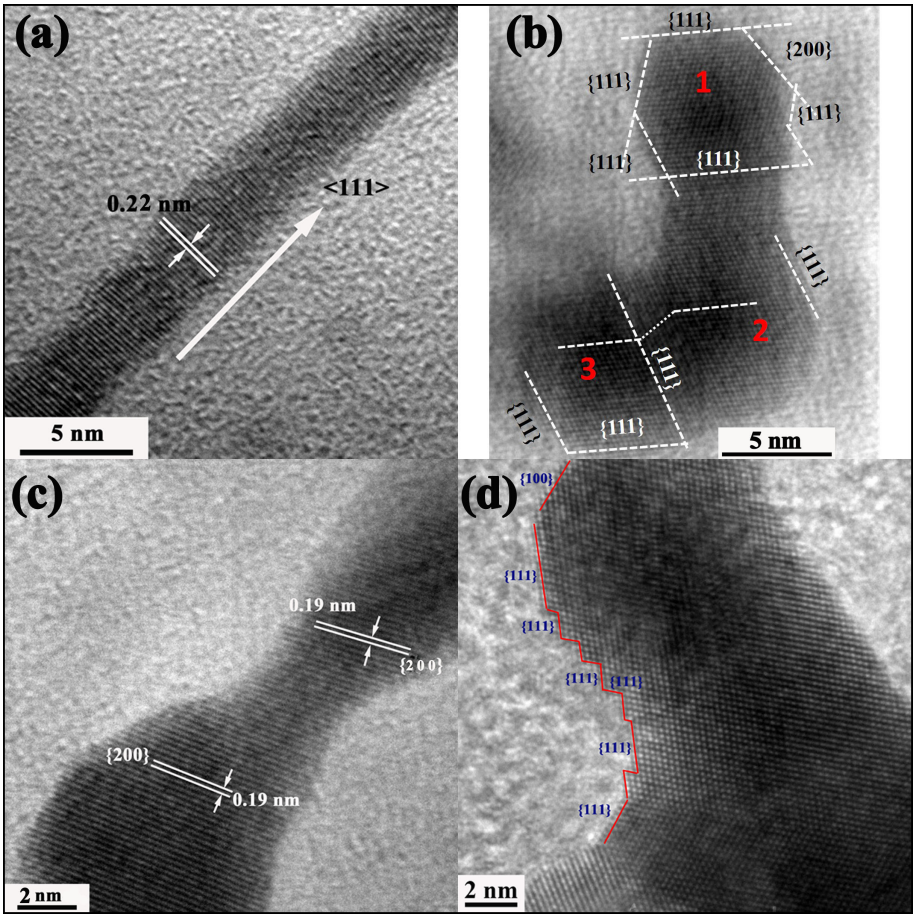

FIGURE 6.9: HRTEM images of Au-Cu nanostructures grown after 2 min. Figures (a) and (c) showing lattice matched attachment along {111} and {200} planes respectively. Figure (b) shows twinning attachment along {111} planes of two crystals. Figure (d) displays facet planes {111} and {100} where another crystal can attach through MA or TA.

most likely adsorb on the various surfaces of NPs to prevent aggregation. Only under the conditions that nanocrystal surface is loosely protected and the van der Waals interaction is strong enough to overcome the capping effect, the surface atoms can then be in direct contact with each other upon the collision between two particles, and may diffuse across the interface to form anisotropic structures. The key factors in determining the formation of nanowires from primary NPs should largely be governed by both the spontaneous exposure of nanocrystal surfaces and the likelihood of bond formation at the interface [40]. The binding strength of capping agents on crystal surfaces can be modeled through calculating the adsorption energy, which is a thermodynamic effect. The effective bond formation, which is a kinetic effect, can be understood based on the surface reconstruction upon the collision between two particles [252].

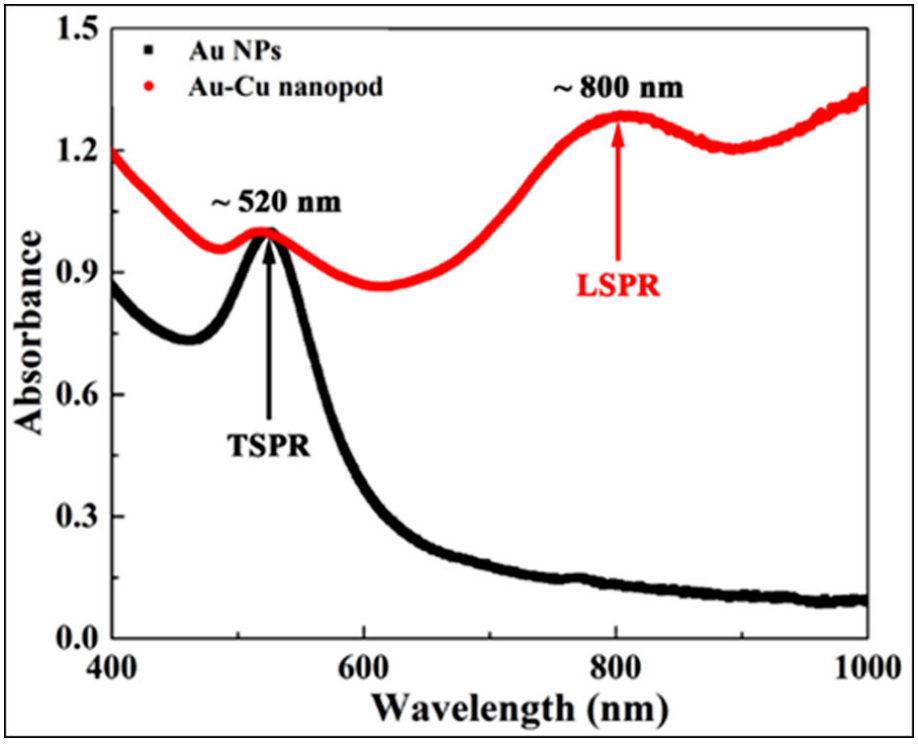

FIGURE 6.10: UV-Vis-NIR spectra of nearly spherical Au NPs and Au-Cu multipods nanostructures.

6.3.3 LSPR behavior of Au-Cu nanostructures

The UV-Vis-NIR absorbance spectra (200 nm -1100 nm) of Au NPs and Au-Cu multipods is shown in the Figure 6.10. The LSPR absorbance maxima λ_{max} corresponding to Au NPs is observed at $\sim$ 520 nm. The LSPR response of Au-Cu multipods shows the presence of a peak in the visible region at $\sim$ 520 nm and a peak in near infra-red region at $\sim$ 800 nm. This drastic red shift in the LSPR peak can be attributed to excitation of higher order multipoles [125]. When concentration of HDA was increased from 45 mg to $\sim$ 90 mg and onwards, no LSPR peak was observed (cf. Figure 6.11 a). As mentioned in the section 6.3.1, morphologies observed from TEM are wire like when concentration of the HDA was 90 mg, 135 mg, and 180 mg respectively. The highly agglomerated nanowires might lead to absence of LSPR peak in 200 nm to 800 nm range. The appearance of LSPR

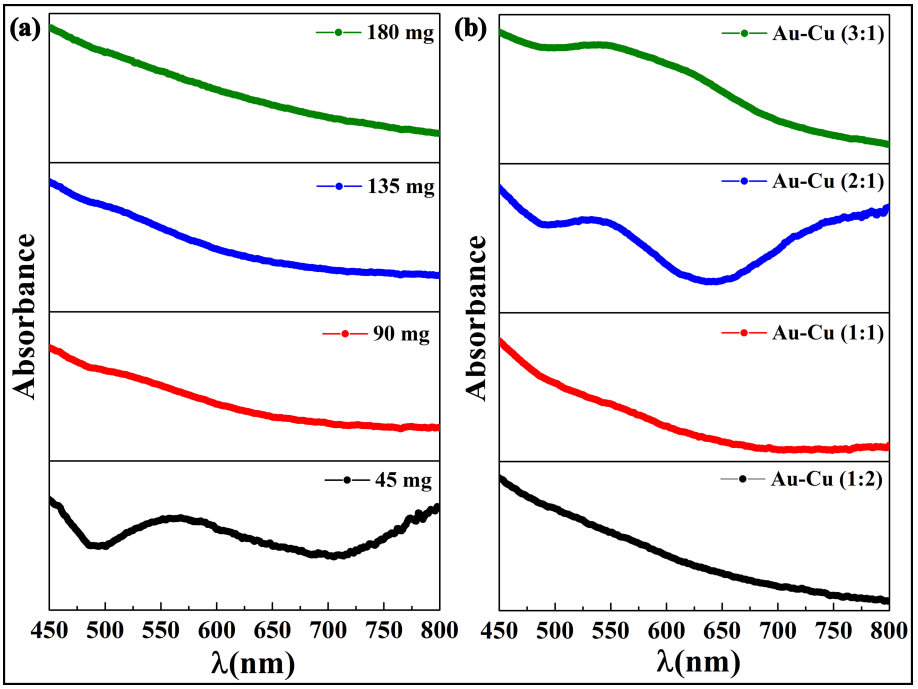

FIGURE 6.11: UV-Vis spectra of Au-Cu nanostructures by varying HDA concentration (a) and Au:Cu precursor ratio(b) respectively.

response similar to HDA concentration of 45 mg has been observed with molar precursor ratio of Au/Cu; 2/1 as shown in Figure 6.11 b.

6.4 Conclusions

Au-Cu nanostructures have been synthesized by wet chemical route wherein $HAuCl_4.3H_2O$ and $CuCl_2.2H_2O$ were co-reduced by glucose in aqueous solution in the presence of hexadecylamine at $\sim 80^oC$. It has been observed that changing the synthesis conditions, nanostructures of various shapes such as nanowires, multiply twinned tripod, tetrapod, etc. were observed. Nanostructures are composed of homogeneous Au–Cu alloy as revealed by STEM-EDS results. The formation of nanowires under the present synthesis condition have been explained in terms of oriented attachment kinetics of Au-Cu NPs. Multiply twinned branched shape Au-Cu (width of branch $\sim$30 nm) products display strong LSPR peak in the near-infrared region ($\sim$ 800 nm) which may provide an avenue for their potential applications in photothermal therapy. This study serves as a template to modulate the LSPR behaviour by controlling the shape and composition for other alloy systems.